

Inmarsat 4F1 Plasma Propulsion System Initial Flight Operations

IEPC-2005-082

*Presented at the 29th International Electric Propulsion Conference, Princeton University,
October 31 – November 4, 2005*

Howard Gray¹

EADS Astrium Ltd, Portsmouth, PO3 5PU, UK

Severin Provost²

EADS Astrium SAS, 31402 Toulouse Cedex 4, France

Michael Glogowski³

Inmarsat Global Ltd, London, EC1Y 1AX, UK

and

Alain Demaire⁴

EADS Astrium SAS, 31402 Toulouse Cedex 4, France

The latest generation of geostationary telecommunications satellites provide increases in power, life and payload mass. For these platforms electric propulsion systems offer attractive overall mass savings, as the propellant gains are significantly higher than any additional hardware mass. The function of the Plasma Propulsion System (PPS) used on the Eurostar E3000 platform is to provide inclination and eccentricity control for north-south station keeping. It is based on the SPT-100 Stationary Plasma Thruster, and in the main exploits hardware already developed and qualified for the French experimental Stentor satellite. This paper presents an overview of the Eurostar E3000 platform PPS as implemented on the Inmarsat 4F1 satellite, along with the in-orbit testing and initial flight operations results.

I. Introduction

Electric propulsion (EP) systems have been advocated for many years for various satellite applications. The large fuel savings they offer compared to conventional chemical propulsion systems (CPS) (a factor in the order of 5 for hall effect thrusters) offers very significant mass savings at satellite level; this technology thereby allows the introduction of large high power satellites within existing launcher constraints. As a result, most satellite prime contractors now offer some form of electric propulsion for their latest large high power platforms, either as a baseline or as an option. It should be noted, however, that there is a penalty in terms of additional hardware mass, making EP particularly useful for satellites which otherwise would have high propellant requirements.

Geostationary telecommunications satellite propulsion systems are typically used for orbit raising and circularisation, north-south stationkeeping, east-west stationkeeping, and attitude control (momentum dumping). The above list is in order of decreasing total impulse requirement. As orbit raising and circularisation normally has to be completed quite quickly (to ensure the satellite can start earning revenue as soon as possible after launch), and

¹ Electric Propulsion Specialist Engineer, howard.gray@astrium.eads.net

² Electric Propulsion Engineer, severin.provost@astrium.eads.net

³ Electric Propulsion Engineer, Michael_Glogowski@inmarsat.com

⁴ Electric Propulsion Group Manager, alain.demaire@astrium.eads.net

as EP typically provides very low thrust levels (less than 1N), its usefulness for primary spacecraft propulsion is limited in this context. Consequently, it has been the north-south stationkeeping requirement which has been the main focus for EP activities, where a high propellant throughput is required but low thrust levels can be accommodated.

EADS Astrium have developed a plasma propulsion system (PPS) based around the Russian SPT-100 thruster for use on their Eurostar E3000 platform^{1,2}, and the Inmarsat 4F1 spacecraft is one of the first commercial exploitations of this. The F1 spacecraft is the first of a series of 3 Inmarsat 4 satellites all of which use identical PPS, and in particular it is the first implementation of PPS on an L-band mobile communication satellite based on the Eurostar E3000 platform. The SPT-100 thruster has extensive flight experience with no reported failures on a number of Russian satellites (in particular, the GALS and Express programmes, and more recently Sesat), as well as a growing number of western spacecraft, and so is considered to be mature with a relatively low residual risk. The European ground qualification for the overall PPS and most of its equipments was largely achieved through the French Stentor programme³, although the loss of that satellite due to a launcher failure means the corresponding in-orbit experience on a European satellite has not been previously available. Ground qualification not provided by Stentor has been achieved through a dedicated EADS Astrium test programme⁴.

II. PPS Description

A. PPS Overview

The function of the PPS is to provide inclination and eccentricity control for North/South station keeping (NSSK) of the satellite. The PPS (shown schematically in Fig. 1) uses Xenon as propellant and includes all devices to store and supply Xenon to the plasma thrusters (four SPT-100), which are accommodated by pairs on two orientation mechanisms (TOM) and which are power supplied by two electronic units (PPU). The PPUs are connected to the Spacecraft Computing Unit (SCU) via a digital 1553B interface, and the TOM is driven by the Mechanical Drive Electronics (MDE) function of the Actuator Drive Equipment (ADE). The pressure regulator valve drivers and pressure transducer power and signal acquisitions are also managed by the ADE. The PPU takes power from the main spacecraft regulated bus.

The PPS feed system comprises a Xenon storage tank (XST), a pyro valve (PV) with its associated Filter (XEF), an electronic pressure regulation system (XRFS), and three fill and drain valves (FDVs); the PPS is then completed by two thruster module assemblies (TMAs) and two power processing units (PPUs), along with their associated pipework and harnesses. The PPS equipments are listed in Table 1.

Each TMA comprises two SPT-100 thrusters and their associated Xenon Flow Controllers (XFC), a thruster orientation mechanism (TOM) bearing and canting the SPTs (with its associated thermal hardware), a set of MLI for thermal control (with a dedicated structure), two Filter Units (FUs, one per thruster), and the associated pipework and harnesses. The TOM and the XFCs are mounted onto an interface base plate (BP), which can be shimmed with respect to the S/C structure. The FUs are directly mounted onto the satellite structure. The TMAs are located approximately midway along the spacecraft Z axis, on the X/Y panel edges, with the thrusters nominally canted at approximately 45°, to ensure the thrust axes pass through the centre of mass of the spacecraft. The TOMs allow the thrust vector to be steered during operation; the TOM steering functionality is handled at ADCS level, driving

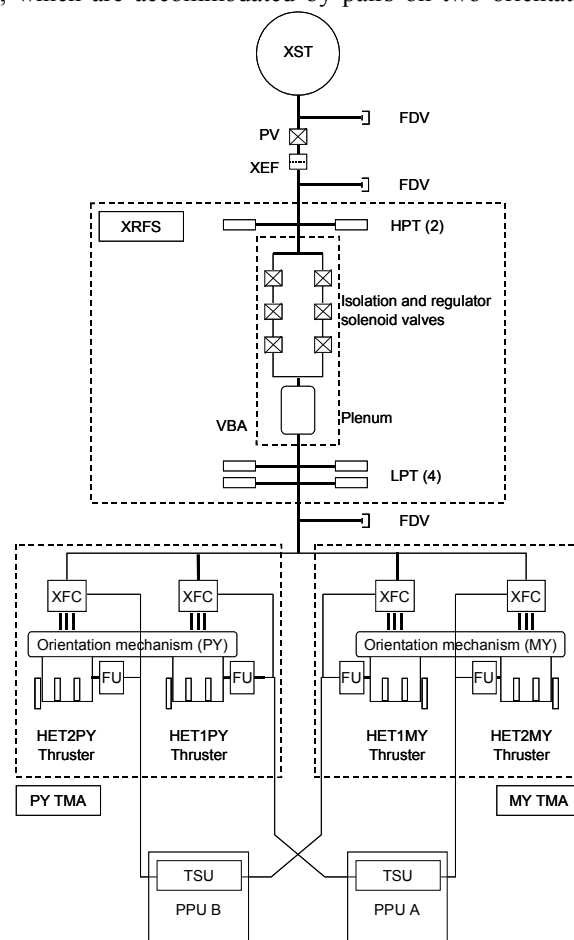


Figure 1. PPS schematic

through the MDE as discussed earlier. Each TOM also has 2 microswitches, which change state at the reference position (one for each axis of movement). Fig. 2 shows the PPS satellite configuration for the TMAs.

The pyro valve isolates the tank from the remainder of the PPS. Tank pressurisation operations are only performed using the FDV placed between the tank and the PV, whereas all the other pressurisation tests are performed using the two other FDVs. After PV firing, the XRFS then isolates the Xenon stored in the XST from the plasma thrusters; during the on-orbit phase, the XRFS supplies Xenon to the TMAs at the required regulated pressure level. The XRFS uses “bang-bang” pressure control, based on the measured downstream pressure; the control function resides in the spacecraft computer, and is achieved via dedicated pressure regulation electronics (PRE).

The validation of the overall flight PPS and interfaces has been achieved by means of rigorous and incremental testing at equipment and spacecraft level⁴, and finally by in-orbit tests prior to flight operations.

Table 1. PPS equipment product tree

Acronym	Title	N° Off
PPS	Plasma Propulsion Subsystem	
— XST	Xenon Storage Tank	1
— PV	Pyro Valve	1
— XEF	Xenon Filter	1
— XRFS	Xenon Regulator and Feed System	1
— HPT	High Pressure Transducer	2 / XRFS
— VBA	Valve Block Assembly	1 / XRFS
— LPT	Low Pressure Transducer	4 / XRFS
— FDV	Fill and Drain Valve	3
— PPSPIP	Pipework (HP and LP)	1 set
— TMA	Thruster Module Assembly	2
— HET	Hall Effect Thruster	2 / TMA
— XFC	Xenon Flow Controller	2 / TMA
— TOM	Thruster Orientation Mechanism	1 / TMA
— FU	Filter Unit	2 / TMA
— N/A	TMA Thermal Device (MLI)	1 set / TMA
— BP	Base Plate	1 / TMA
— N/A	TMA Pipework	1 set / TMA
— N/A	FU - HET Harness (HIB)	1 set / TMA
— PPU	Power Processing Unit (with TSU)	2
— EMH	PPU - TMA Harness	1 set



Figure 2. Inmarsat 4 satellite configuration

B. PPS Operation

1. HET Operation Overview

The SPT-100 HETs are plasma thrusters using Xenon as propellant with a high thrust density. The thruster consists of the following major elements (see Fig. 3 below):

- The anode gas distributor is a metallic annular assembly, which provides uniform Xenon distribution into the chamber through a series of small orifices. The anode gas distributor and the propellant feeding line are at a potential of +300 Volts during the discharge, and are isolated from the inlet gas supply line through two redundant electrical isolators
- The discharge chamber is an annular U shaped canal made of a ceramic Boron Nitride and Silicon Dioxide mix, which insulates the thruster body from the plasma
- The magnetic system consists of a single internal and four external electromagnetic coils which are electrically fed in series with the discharge, and of a magnetic permeable path unit to produce the radial magnetic fields in the discharge chamber

Two redundant cathode assemblies are located outside the thruster body, each of which includes:

- A getter which traps all the oxygen traces in the Xenon before feeding the high temperature core
- Heating coils used during start-up phase to bring the device to the necessary temperature
- A Lanthanum Hexaboride thermal emitter which, when heated to a high temperature, ensures electron emission
- Thermal screens positioned around the high temperature cathode core, to thermally protect the casing and thermally control the cathode
- An ignitor used to initiate the discharge

The plasma is created within the discharge chamber by means of electron bombardment of the neutral xenon gas. The electron source is the hollow cathode located outside the thruster exit plane. The two cathodes are provided in

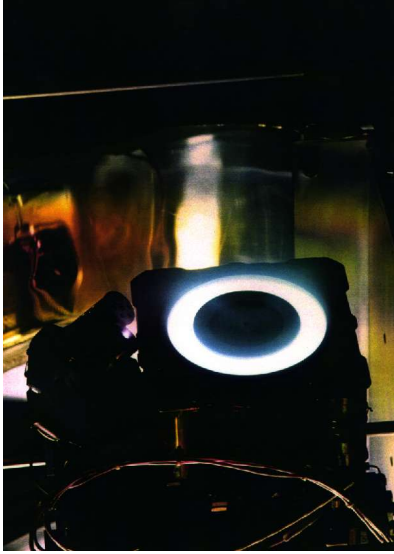
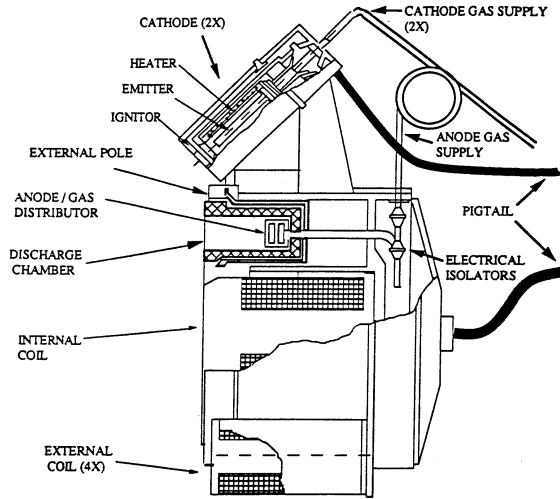


Figure 3. SPT-100 Thruster



the SPT-100 design for redundancy, but only a single cathode is used during operation. The free electrons emitted by the cathode are attracted to the 300V potential which is applied to the anode located at the bottom of the discharge chamber. These electrons, once in the discharge chamber, are subjected to the radial magnetic field and become “trapped” in spiral paths. They then collide with the xenon gas particles, which are introduced to the discharge chamber through the anode injector orifices. This results in the creation of positively charged xenon ions within the discharge chamber, which are then subjected to the potential difference of approximately 300V between the anode and the exit plane of the thruster, and are thus strongly expelled from the thruster.

The neutralisation of this positive ion beam is performed by the hollow cathode. Electrons supplied by the cathode are naturally attracted to the positive ion beam; this is a self-regulating process with no need for active external control. The same hollow cathode is used to provide both the electrons for the main discharge plasma and the neutralizing electrons.

2. *Thruster Control*

The overall operational sequence of the PPS is controlled by the spacecraft on-board software, via the PPU. Each PPU controls the selected SPT and its associated XFC on the basis of programmed procedures and commands received from the on-board computer.

The XFC (shown in Fig. 4) consists of valves, filters and a thermally constricting capillary tube (thermothrottle) in series with flow restrictors to control the propellant flow ratio between the operating cathode and the anode unit. The XFC modules provide independent flow paths for the anode and for each cathode. On each flow path, two valves in series are provided. The PPU provides a closed loop Xenon flow regulation to the thruster by adjusting the thermothrottle current; the density and viscosity of the gas are varied in order to keep a constant delivered mass flow rate, and so the discharge current is maintained at its nominal set value (which maintains a fixed nominal thrust level).

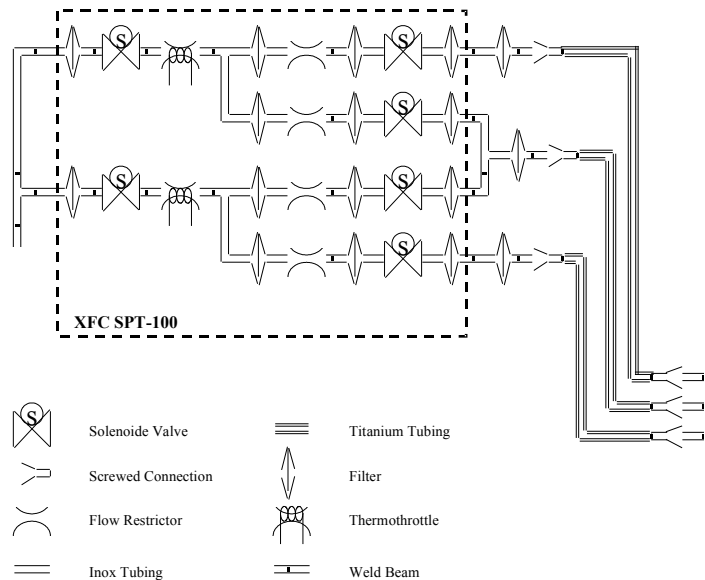


Figure 4. XFC Schematic

Each PPU supplies a pair of SPT-100 thrusters (and their associated XFCs) with electrical power to enable their correct operation. The Thruster Selection Unit (TSU), which is included in the PPU, is a switching unit receiving all

PPU outputs and transmitting them to one of two thrusters; each PPU can only operate one thruster at a time. The PPU is provided by ETCA.

The PPUs exchange data with the on-board computer. According to the received orders the PPU enters into one of its six possible modes: OFF, STAND-BY, CONFIGURATION, VENTING, AUTOMATIC and REMOTE. These transitions are as follows (see Fig. 5):

After the DTC (direct telecommand) “PPU ON” to turn ON the PPU DC/DC, the sequencer enters into an initialisation phase before being put in stand-by mode.

In the “OFF” mode the only acceptable command by the PPU is the ON command which puts the internal micro-controller into the “STAND-BY” mode.

In the “STAND-BY” mode, only low level electronics are active. The PPU then accepts any transition to another mode.

In the “CONFIGURATION” mode the PPU accepts orders to modify the selection of SPT and XFC units by actuating the TSU relays. It is also possible to modify the setting of firing parameters.

The “VENTING” mode is only used at the mission beginning to allow venting of the Xenon lines before the first SPT firing. In this mode the PPU opens all the XFCs valves on the selected thruster.

In the “REMOTE” mode the PPU micro-controller can be overridden by dedicated commands. The on-board computer allows “step-by-step” management of the thrusters in order to provide flexibility to the ground operators if necessary.

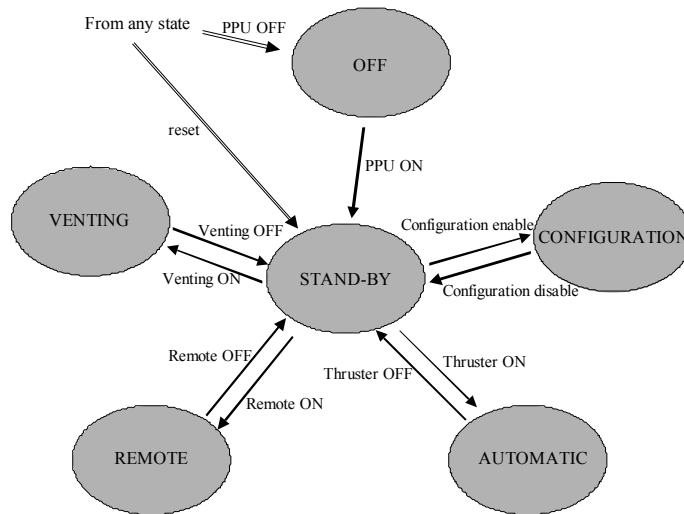


Figure 5. PPU States

The “AUTOMATIC” mode is the nominal mode of the PPU when the PPU drives the firing SPT in closed-loop. The power supplies of the PPU are active. The firing is driven with the set of parameters defined in the configuration mode. The logic of the “AUTOMATIC” mode is as follows:

- During the starting phase, the PPU sequences as follows:
 - Heat the selected cathode and thermothrottle up to the corresponding stabilised thrust level for the SPT
 - Open the XFC valves
 - Supply the cathode with ignition pulses once the Xe flow is stabilised
- The SPT has to be started within a given delay period from the start of this sequence. In case of failure the PPU goes into “STAND-BY” mode and sends a failed status signal
- During the stabilised phase (after SPT starting), the initiator electrode is no longer supplied and the closed control loop becomes operational. In stabilised mode the discharge current control is made by adjusting the Xenon flow rate through the thermothrottle in the XFC

3. XRFS Operation

The XRFS is a generic product based on the Electronic Pressure Regulator Mechanism (EPRM) qualified and delivered by EADS Astrium for ESA’s Artemis satellite. It has been designed to be able meet the requirements of a wide range of potential applications⁹.

The XRFS can be in Off, Stand-By or Regulating mode; when in Off mode it is completely unpowered, and when in Stand-By mode the pressure transducers are powered and pressure TM is available. All XRFS operations are performed in Regulating mode; in this mode, one of the two parallel valve branches is operated by the pressure regulation electronics (PRE) under the control of the spacecraft computer. During regulation, the two upstream isolation valves are held open continuously, and the downstream valve is pulsed as described below.

The XRFS pressure regulation is achieved by means of a closed loop control. The spacecraft computer continuously reads the low pressure transducers information, and calculates the effective plenum pressure based on a majority vote and averaging scheme. It then sends a valve open command to the regulation valve when a pre-defined lower threshold is reached, and similarly a valve close command when an upper threshold is reached. The regulation thresholds have been selected to minimise the number of regulating valve pulses ,whilst simultaneously limiting the pressure ripple resulting from the Xenon filling and then draining from the XRFS plenum.

Before each manoeuvre, an initialisation phase is required to be sure that the pressure at the XFC inlet is in the correct range at the beginning of the thruster firing. It should be noted that between two manoeuvres, the thruster inlet pressure can decrease or increase out of the specified range mainly due to thermal environment variations. Hence before each manoeuvre, the low pressure in the plenum is measured and compared to pre-set initialisation thresholds. If the measured plenum pressure is outside the range of these thresholds, a filling or venting activity is performed to bring the pressure back into the specified pressure range.

In addition to the above thresholds, pressure monitoring limits are implemented in the software to prevent the XRFS from any over- or under-pressure failure. In the event that any violation of these pressure limits is detected, the software will stop the regulation. The PRE also includes a hardwired overpressure protection (at a slightly higher pressure level), which will automatically close the valves in the event that software fails, or communications with the spacecraft computer are interrupted. In the event of power loss, the valves will all close automatically.

C. PPS/Spacecraft Interactions

HETs produce both highly energetic and charged particles, with a non-negligible ion flux at high angles from the thrust axis. This raises several potential interactions with the surrounding surfaces of the spacecraft:

- Dynamic effects
- Erosion and contamination of sensitive surfaces
- Spacecraft charging modifications
- Radio-Frequency perturbations

Some of those interactions may have non-negligible impacts at system level (dynamic effects must be managed by ADCS, erosion and contamination may lead to thermo-optical properties degradation over life, etc.). EADS Astrium has developed a set of modeling tools to assess the main effects of PPS at system level⁵. These tools have been developed in the frame of the generic Eurostar E3000 platform programme, and used to perform PPS / spacecraft interaction analyses for the Inmarsat 4F1 specific configuration.

1. Plume flow-field

This has been computed with the *MC2DP* modeling tool, based on a hybrid Particle In cell (PIC) / Direct Simulation Monte Carlo (DSMC) code⁶. The results from this code (Xenon ion current and energy in the plume) have been compared with both on-ground and in-flight measurements and show good correlation. Uncertainties still remain in the area of high divergence angles (typically 80° from the thrust axis and beyond, where most interactions occur), which imposes the need to use conservative assumptions in this area.

2. Dynamic effects

These have been computed with the *PIONIC* tool. The direct impingement of the undisturbed flow-field is computed using the Schaaf-Chambre model. The computation of the reflected flow and further impacts (if any) is carried out with a Monte Carlo ray-tracing technique, based on the knowledge of normal / tangential / energy accommodation coefficients. These coefficients have been evaluated from data from the GALS satellite; in the near future, they will be updated from in-orbit data from Eurostar E3000 satellites.

3. Erosion and contamination

These have been computed with the *CIONIC* tool. An erosion and contamination test campaign carried out at ONERA / DESP has allowed enhancement of this tool with an accurate sputter database⁷, covering the following aspects:

- Characterisation of the sputtering yields for several space-specific materials (Kapton, paints, cover-glasses, etc.), for various Xenon ion energies and incidences
- Characterisation of the thermo-optical degradations for a given eroded thickness
- Characterisation of the re-emission profiles for eroded products (contamination tests with Quartz Controlled Microbalances). This allows definition of both diffuse and pseudo-specular re-emission lobes
- Characterisation of the thermo-optical degradation for a given deposited thickness (i.e. after contamination)

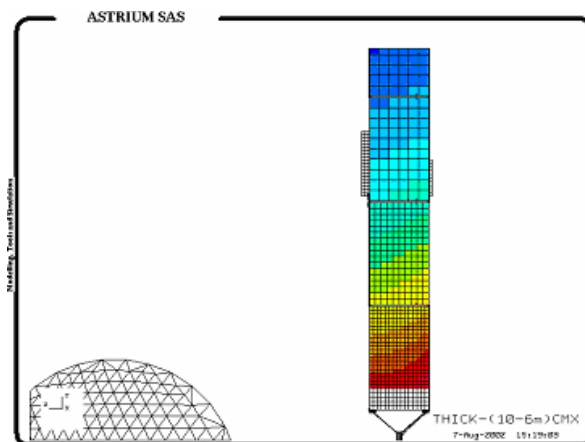


Figure 6. Solar array erosion results on Inmarsat-4 F1

Fig. 6 provides an example of solar array erosion prediction results for Inmarsat 4F1.

4. *Spacecraft charging*

PSPICE simulations have been carried out to infer the spacecraft potential equilibrium when the PPS is used (refer to Fig. 7). The thruster power supply (cathode to anode voltage) is floating with respect to the satellite ground, and the cathode naturally stabilizes to a slightly negative potential with respect to the space plasma (in the region of -19V, based on Smart-1 flight experience⁸). The rest of the satellite is then allowed to float with respect to the cathode. This then stabilises to a voltage where the current from the impact of ions just balances the current from the impact of electrons. As the electrons are lighter and thus more mobile, a slightly positive surface attracts as much electrons as a larger surface at a much lower negative potential. This drives the dielectric surfaces to the “plasma floating potential” in this high density, low electron temperature plasma.

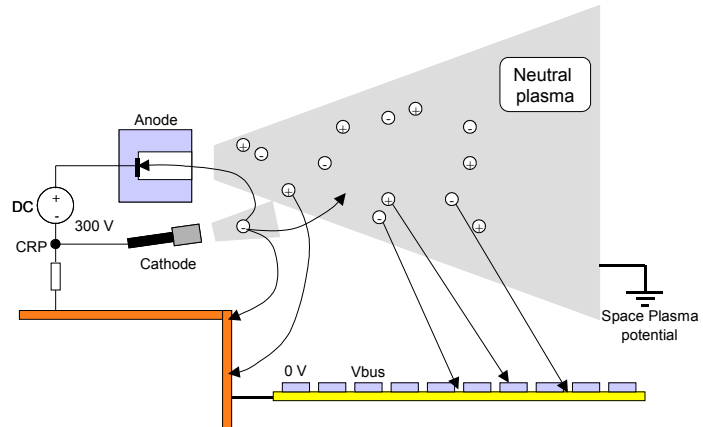


Figure 7. Charge transfer by the PPS

Regarding the satellite structure, the contact with the plasma is very dependant on the solar array interconnects which are conducting surfaces, with a direct contact to the plasma and a low impedance path to the ground. The potential of the interconnects with respect to the satellite ground varies from approximately 0V at one section end to V_{bus} at the other end. The balance condition occurs when a slight interconnect area is left at a slightly positive potential with respect to the space plasma; that area then attracts enough electrons to compensate the ions impacting the rest of the interconnects. Such a phenomenon drives the spacecraft ground potential between floating potential to $-V_{bus}$. As a result of this, the CRP (Cathode Reference potential) should stabilise to approximately:

$$CRP = V_{cathode} - V_{S/C} = (V_{cathode} - V_{plasma}) - (V_{S/C} - V_{plasma})$$

The cathode to plasma potential has already been estimate to be of the order of -19V (see above); the spacecraft to plasma potential can be between 0V and the bus voltage (nominally 50V), depending on the level of plasma connectivity to the solar array interconnects. Consequently, the CRP is estimated to take values between -19V and +31V. This is consistent with the in flight results described below (taking into account the TM saturation for high positive values).

RF interactions: A computer tool has been developed based on ray-tracing methods. The RF wave propagation through the plume is modeled by rays, each ray carrying information on the EM field intensity, phase and polarisation. Rays are tracked within the plume and refracted (the refraction index being function of electron density and its gradients). Finally rays are collected on an exit plane in a low-density region, and EM fields are computed on this exit plane. This allows retrieval of all the characteristics of the perturbed RF signal (amplitude and phase antenna diagram, in co- and cross-polarisation).

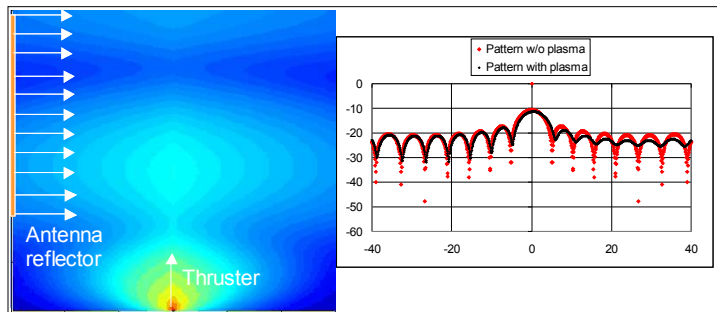


Figure 8. Example of perturbed antenna pattern (note that the configuration is not representative of Inmarsat 4)

An example of the simulation, with the resulting perturbed antenna amplitude diagram (in an non-representative thruster / antenna configuration, however), is shown in Fig. 8.

5. *Application to Inmarsat 4F1*

All the above analyses have been carried out for the Inmarsat 4F1 configuration, and accounted for in the system design of the satellite (ADCS, power and thermal budgets). These interactions were also investigated during the initial flight operations, as discussed in the following sections of this paper.

To improve the modeling methods for future satellites embarking HETs, it is foreseen to correlate these results with in-orbit data from Inmarsat 4F1:

- Dynamic effects (torques TM), spacecraft charging (CRP TM) will allow the correlation of some macroscopic information of the plume model
- Other effects such as erosion, contamination and associated thermo-optical degradations are longer term effects that will not be noticeable for several years

III. Initial Flight Operations

A. Operations Sequence

Inmarsat 4 was launched from Cape Canaveral on 11 March 2005 aboard Atlas 5. Following the successful launch of the satellite, the PPS was initialised and tested in orbit. This sequence included the following steps:

- Xe storage and regulation system health checks (pressure and temperature monitoring)
- Release of the pointing mechanisms, and check of successful release by motion checks
- Venting the low pressure section of the PPS in order to expel any contaminants, and refilling with flight-quality Xenon
- Firing each thruster and cathode combination

Eight firing tests were performed in total (two for each thruster, with the prime and then redundant cathode); both the prime and redundant branch of the regulation system were also used during this test programme. Six of the firings were 30 minutes in duration, with 2 firings of 2 hours each (these timings are approximate; the precise durations are given in Table 5 below).

The Eurostar E3000 platform allows a number of telemetry channels to be acquired at high frequency; this enables a reasonably well detailed investigation of the thruster start-up transients in the real space environment, as discussed below.

B. Initial In-Orbit Operations Results

1. TOM Release

TOM unlocking occurred on 29th March 2005. Each TOM was successfully released by firing the prime and redundant initiators simultaneously on each pyro release device in turn (there are 2 pyro release devices on each TOM).

This was then followed by a reference position search, looking for the optical microswitch state changes as the TOM is moved. This ‘‘TOM reset’’ procedure drives the TOM back to its reference position, following a dichotomy-like algorithm. This activity clearly demonstrated that TOM release has been successful as follows:

- The release of both TOMs was confirmed by the change of state of the 2 optical switches for both TOMs
- The reference position of both TOMs was reached, within less than 60 actuator steps compared to the predictions (corresponding to an angular error less than 5’)

2. Xe System Health Check

The Xe feed system was checked immediately prior to PPS venting and initialisation (see below), with the results as shown in Table 2. All values are in the expected range, confirming the good health of the feed system prior to any PPS operations.

It should be noted that the pressure levels are strongly dependent on the tank temperature; this correlation was tracked and compared with values immediately before and after launch, which confirmed that there were no unexpected pressure excursions.

3. Venting and XRFS Initialisation

This activity was performed on 30th March 2005, starting at approximately 09:00 GMT. The vent proceeded in 4 stages, venting through each thruster in turn. The total vent duration was approximately 8 hours, to ensure:

Table 2. Xe system initial health check

Parameter	Pass / fail criteria		Result
	Min	Max	
XRFS prime temperature	14	63	41.0
XRFS redundant temperature	14	63	37.6
XRFS temperature difference	-6	+6	2.4
HPT1	68	88	75.15
HPT2			75.12
HPT difference	-3.21	+3.21	0.03
LPT1	2.5	3	2.67
LPT2			2.68
LPT3			2.67
LPT4			2.68
LPT difference	-0.07	+0.07	0.01

- (a) Adequate purging through each XFC
- (b) Exposure of the low pressure pipework to a hard vacuum, to evacuate any residual potential contaminants)

This activity was completed with the priming of the LP section, which was achieved by placing the XRFS into regulation mode. This initialisation sequence brought the LP section pressure slowly back up to 2.5 bar; the peak pressure in the LP section indicated that the XRFS operation resulted in a pressure overshoot of just 20 mbar. This initialisation with the XRFS is characterised by a the pressure rise which is slower, smoother and more readily controlled than that which can be achieved with mechanical regulators.

The pressure transducer and thermistors were checked for consistency throughout the above operations; all readings were within the range of measurement accuracy, as detailed in Table 3. The Xenon tank pressure and temperature conditions were also recorded during this activity; no significant trend in tank conditions was seen during the venting.

Table 3. Pressure and temperature consistency during vent

Parameter	Pass / Fail criteria		Results	
	Min	Max	Min	Max
XRFS temperature difference (°C)	-6	+6	0.0	4.0
HPT difference (bar)	-3.21	+3.21	0.00	0.16
LPT difference (bar)	-0.07	+0.07	0.00	0.02

4. Initial Thrust Firings

The test consisted of firing each of the 4 thrusters using prime and then redundant cathodes. The sequence of the firings is detailed in Table 4.

Table 4. Initial thruster firing sequence

Firing	Date and Time (GMT)	Thruster	Thruster position	PPU	Cathode	XRFS branch in use
1	31/03/05 06:40	#85	HET1PY	A	A	Prime
2	31/03/05 13:41	#87	HET1MY	B	A	Redundant
3	01/04/05 06:26	#85	HET1PY	A	B	Redundant
4	01/04/05 13:41	#86	HET2PY	B	A	Redundant
5	01/04/05 18:41	#104	HET2MY	A	A	Redundant
6	02/04/05 08:06	#86	HET2PY	B	B	Prime
7	02/04/05 13:41	#104	HET2MY	A	B	Prime
8	02/04/05 17:16	#87	HET1MY	B	B	Prime

All these in orbit test (IOT) firings were completed successfully, with no unexpected behaviour. The results for all 8 firings were similar; curves illustrating the main performance characteristics for firings 2 and 8 (up to 75 minutes out of approximately 2 hours operation for firing 8) are shown below.

A number of points are of particular interest:

- The cathode on each thruster is electrically floating, but during thruster operation is tied to the external plasma conditions; measurement of the cathode reference potential (CRP) then gives some indication of the environment potential of the spacecraft. In general, the CRP was positive, although negative values were also seen on a number of firings (as discussed further below), and occasionally the TM was saturated (this can be seen in the results for firing 8 shown below).
- For a few minutes after thruster ignition, there is a significant level of current fluctuations on a number of the telemetries, in particular the discharge current and thermothrottle current (as can be seen below); this is associated with out-gassing of the thruster ceramic, and is a well-known phenomenon seen from previous ground test and flight data.
- The duration and amplitude of initial transients were seen to be decreasing from the beginning to the end of the IOT, indicating a near completion of out-gassing activity. This outgassing is completed within 3 hours of firing for each thruster.
- Throughout each firing, the telemetry has enabled the calculation of the thrust, flow rate and specific impulse. The thrust and flow rate are shown in the curves below; it can be seen that the flow rate in particular has to be treated with some caution during the initial out-gassing.
- There are transients in the anode and thermothrottle currents, which translate into transients in thrust and flow rate; these result from the pressure transient coming from the XRFS regulation (the synchronization of these transients with the pressure profile can be clearly seen in the graphs below). They are in line with pre-flight predictions, in terms of magnitude, synchronization and duration, and are well within the acceptable

limits. The performance transients are of a sufficiently small duration and magnitude that they have negligible impact on the average thrust and specific impulse over a complete firing. This behaviour is comparable to that seen from the extensive Russian flight experience.

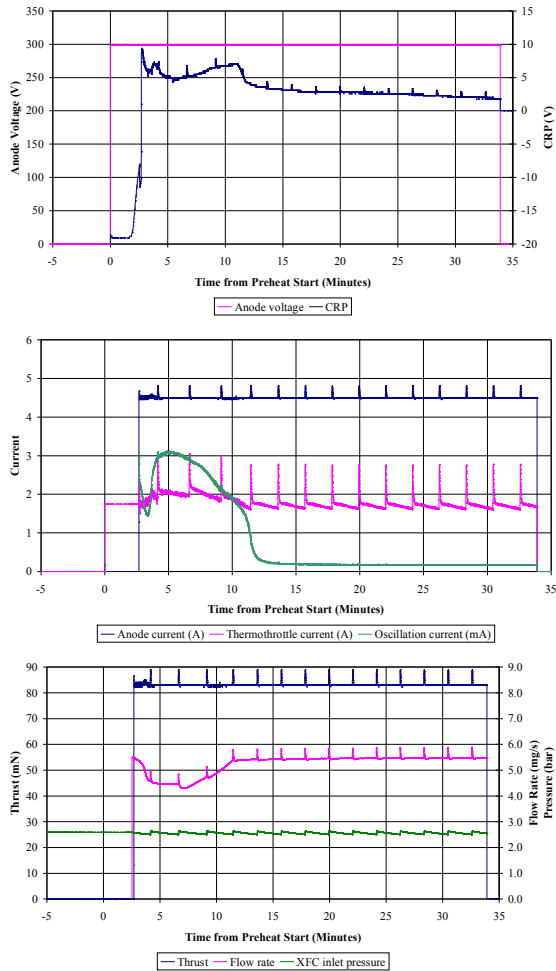


Figure 9. Firing 2 results and performance

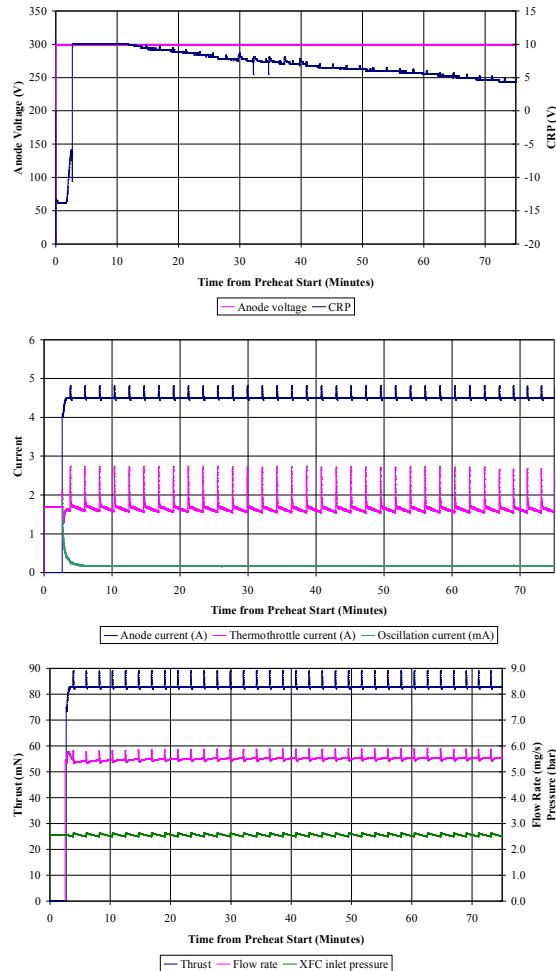


Figure 10. Firing 8 results and performance

The disturbance torques induced by the PPS firings were found to be small and easily managed; around 2 axes these were cancelled by suitably trimming the TOM movements, and around the third axis (for which the TOM cannot provide any trimming) the small torque levels seen were managed by wheel off-loading

In addition to the above, all other PPS TM have been checked for all the above firings; no unexpected values have been seen.

The performance figures and firing timing data for all 8 firings are shown below, along with the corresponding thruster acceptance test data for comparison. The in-orbit data can be seen to correlate well with the equivalent ground test data; the maximum discrepancies are 0.12mN thrust and 40s specific impulse (which should be compared with allowable tolerances of 3.2mN and 96s on thrust and specific impulse respectively due to the modelling and TM errors); hence all the in-orbit test data can be considered to be well within the allowable tolerances compared to acceptance tests.

Table 5. Thruster performance summary

Thruster		Firing	Cathode	Firing time (min)			Average over run		Average stabilised		Acceptance test	
Location	Serial no			Total	Outgas	Stabilised	Thrust	Isp	Thrust	Isp	Thrust	Isp
HET1MY	#87	2	A	31.2	8.7	22.5	83.30	1617	83.31	1556	83.3	1578
		8	B	131.2	3.2	128.0	83.08	1535	83.10	1535	83.1	1575
HET2MY	#104	5	A	31.2	10.0	21.2	82.75	1562	82.76	1529	82.8	1569
		7	B	31.2	5.7	25.5	82.10	1541	82.17	1531	82.2	1557
HET1PY	#85	1	A	31.2	8.7	22.6	83.84	1599	83.88	1567	83.9	1596
		3	B	131.2	5.0	126.2	83.43	1574	83.45	1571	83.5	1585
HET2PY	#86	4	A	31.2	8.4	22.8	83.01	1572	83.00	1552	83.0	1581
		6	B	31.2	2.2	29.0	82.98	1586	83.07	1591	83.1	1589

5. System Interactions

PPS to Electrical Power System (EPS): The Inmarsat 4 electrical power system employs two buses for directing solar array current to the various satellite loads. Each PPU can be connected to either bus and, in turn, can draw power from either solar array. The PPS and electrical power system configurations are summarized in Table 6 for the above 8 firings. It identifies the power supply regulation unit (PSR) and solar array wing for the selected PPU and SPT. It also includes the average position of the solar array during the firing and the cathode reference potential at the end of the firing. The solar array angle varied by $\pm 7.7^\circ$ for the 30 minute firings and $\pm 33^\circ$ for the 130 minute firings. Of the 8 firings four were performed with plume impingement directly onto the solar array wing that was providing current to the PPU to drive the plasma thruster. The other four were performed with plume impingement onto the opposite wing from the one providing power to the PPU.

Table 6. Summary of PPS & EPS configuration during IOT firings

Firing	Thruster position	PPU	PSR	SA	Impingement	+Y Angle (°)	- Y Angle (°)	CRP (V)
1	HET1PY	A	1	+Y	Active	23.23	340.57	7.82
2	HET1MY	B	2	-Y	Active	128.8	235.62	2.02
3	HET1PY	A	1	-Y	Active	32.32	331.69	5.71
4	HET2PY	B	2	-Y	Inactive	128.93	235.58	-1.68
5	HET2MY	A	1	+Y	Inactive	203.81	160.39	-0.62
6	HET2PY	B	2	-Y	Inactive	44.98	319.26	3.60
7	HET2MY	A	1	+Y	Inactive	129.18	235.56	-4.32
8	HET1MY	B	2	-Y	Active	195.21	169.14	5.18

The cathode reference potential (CRP) provides a measure of coupling between the thruster plasma and power system via the solar array interconnects (as described above). The greater the coupling between the plasma and solar array, the more negative will the power system ground become. Since the CRP is fixed at one end to the space plasma potential and varies with the satellite ground on the other, the CRP value will tend to become more positive with greater solar array coupling. Fig. 11 depicts the CRP evolution for firings 2, 5, 7 and 8. For each of these firings the CRP value is similar to the ground measured CRP when cathode heating begins (start of low-level electron emission) and before thruster ignition occurs. At ignition the CRP rises rapidly as the SPT plasma expands around the solar array and interacts with the power system.

Firings 2 and 7 were performed with the -Y TMA at similar solar array angles except that plume impingement occurred on the active solar array for firing 2 and on the inactive solar array for firing 7. This configuration has a noticeable effect on the coupling between the plasma plume and power system based on the higher CRP value for firing 2 (2.02V) than that of firing 7 (-4.32V). This difference is very likely due to the fact that the inactive solar array is at a lower average cell voltage as a consequence of a higher level of cell string shunting. The difference in CRP values for firings 2 and 8 and for firings 5 and 7 highlights the effect of solar array angle on plasma coupling with the array.

The CRP TM shows that the cathode potential stabilises at a lower positive potential (typically a few volts) than predicted, this stabilised potential depending on solar array position. This could be due to one or both of the following:

- Ion current collected by the solar array interconnects has been over-estimated in the above analysis
- Current collection by the thruster casing itself (grounded by a low impedance). This collection happens in the thruster vicinity and is thus subjected to high uncertainties.

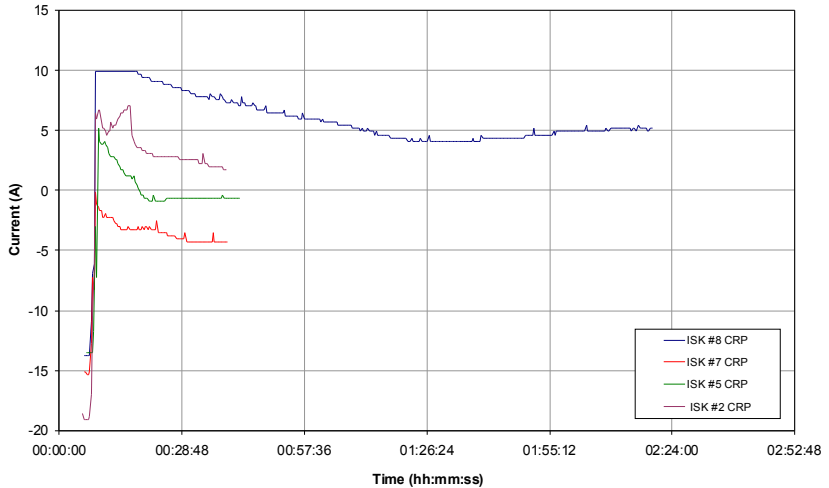


Figure 11. Comparison of CRP for four different PPS and power system configurations

Comparison of the CRP theoretical predictions with in-flight measurements will be subject of further future study.

The change in bus, shunt and PPU currents during a firing can be seen in Fig. 12 for firing #7. The currents appear quite stable, and comparing the average current values at the start and end of the firing yield a difference of +0.05A for bus current, +0.083A for PPU input current, and +0.155A for shunt current.

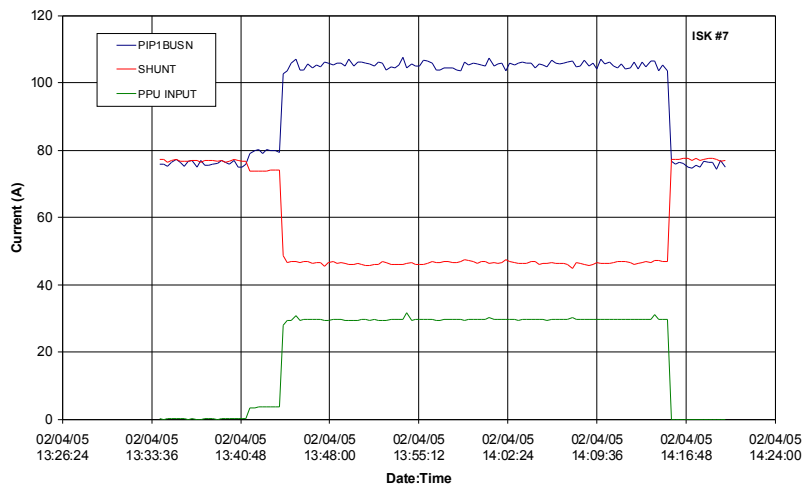


Figure 12. Comparison of bus, shunt and PPU input currents during firing 7

PPS to TT&C System: The first 2 firings provided an opportunity to assess whether there was any effect of the thruster RF emissions on the telecommand receive (TCR) function. During these firings the payload was undergoing the switch-on sequence and likewise, receiving several commands from the ground station. Any effect would have been manifested in irregular fluctuations in the TCR gain. No effect was observed during ignition or steady-state operation for both thruster firings. Antenna gain telemetry showed no variation from the nominal value, and satellite commanding proceeded with no anomalous events.

PPS to ADCS Sensors: No impact of thruster plume emissions (optical or plasma) on ADCS sensor functionality has been observed during the 8 manoeuvres; this behaviour is completely in line with the corresponding system analyses.

6. Summary of In-Orbit Test Results

All in-orbit tests were successfully completed, with all the data analysed and shown to be as expected within the limits of the TM accuracy.

Throughout each firing, the telemetry has enabled the calculation of the thrust and specific impulse. These figures were found to correlate well with the equivalent ground test data, with all the differences being well within the tolerances arising from the telemetry and ground testing accuracies.

C. Operational Use of PPS

1. PPS Operational Performance

Two additional manoeuvres (firing #9 and #10) were performed 36 hours apart from each other with the nominal pair of thrusters for the nominal firing duration. Each thruster had been operated for an extended period of time prior to these two firings, so out-gassing was not expected to contribute to thruster performance. Firing #9 was performed with HET1MY using PPU B. The burn duration was 125 minutes and had very repeatable maximum pressure levels on the XRFS. The discharge current oscillations decreased to 0.177 mA within 60 seconds of start of firing, implying that the out-gassing of this thruster is well advanced. Firing #10 was performed with HET1PY using PPU A. It too was completed without any incidence and had very repeatable maximum pressure levels on the XRFS. The burn duration was 123 minutes, and discharge current oscillations reduced down to 0.213 mA within 71 seconds of start of firing. Table 7 summarizes the performance parameters of the two thrusters used during these performance determination manoeuvres. The first set of data is directly from the unit acceptance test (AT) data; the second set represents the flight performance data computer from the TM. The discrepancies are all within the TM accuracy; the worst case discrepancy is 3.3% on the flow rate, which has to be compared with a tolerance of 4.7% arising from the TM and data reduction errors.

Table 7. SPT-100 Operational Performance Parameters

	Firing #9			Firing #10		
	AT	Flight	Diff	AT	Flight	Diff
Anode voltage (V)	300	298.6	-0.5%	300	298.6	-0.5%
Anode current (A)	4.5	4.500	0.0%	4.5	4.498	0.0%
Thermothrottle current (A)	1.72	1.696	-1.4%	1.73	1.743	+2.8%
Flow rate (mg/s)	5.38	5.559	+3.3%	5.36	5.515	+2.5%
Thrust (mN)	83.3	83.301	0.0%	83.9	83.862	+0.7%
Specific impulse (s)	1578	1545.3	-2.1%	1596	1554.4	-2.6%

Fig. 13 illustrates the measured performance parameters during the last 30 minutes of firing #10, which show almost identical behaviour to firing #9 and the in-orbit test plots shown above.

Overall, the computed performance parameters are consistent with the ground EIDP values and fall within the tolerances identified above. Using the steady-state specific impulses (1578s and 1596s) and mass flow rates (5.38 mg/s and 5.36 mg/s) for prediction of the NSSK manoeuvre requirements, the two manoeuvres achieved a small over-performance of +2% and +0.4% with respect to the planned delta-V. These results have been used to confirm the PPS capability to support the Inmarsat 4 mission life requirements.

2. Nominal PPS Operations

Since the in orbit tests and two firings for PPS performance verification, over 50 SPT-100 manoeuvres have been executed on Inmarsat 4F1 for control of satellite inclination and eccentricity during normal operations. The N/S efficiency, which is defined as the ratio of actual delta V and planned delta V, has converged to approximately 99% through small adjustments in the overall station-keeping manoeuvre plan. This optimisation activity is expected to continue through the first year of mission life, as the Inmarsat operations team becomes more familiar with the satellite performance during PPS firings. The total accumulated firing time is currently in excess of 100 hours, or over 50 hours per nominal thruster.

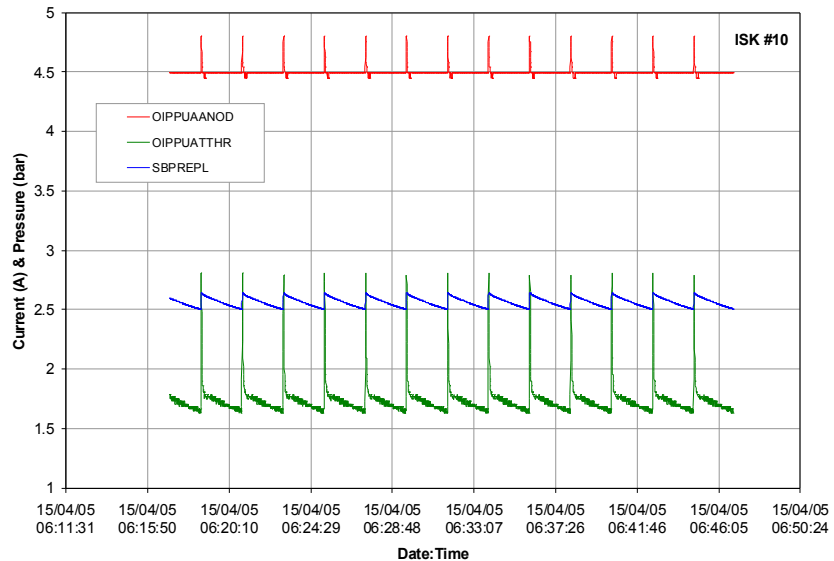


Figure 13. SPT-100 measured performance parameters during last 30 minutes of firing (anode current, thermo-throttle current and plenum

3. *PPS/Payload Interactions*

The two firing manoeuvres performed for thruster performance verification coincided with the payload in-orbit test activity. Efforts were made by the payload test team to assess whether the operation of the SPT-100 and its plasma plume environment produced any noticeable effect on the overall payload performance. Both return phase noise and return C/No tests were run during and after plasma firing. No performance change was observed. Other effects, such as beam steering or thruster EMI on the down-link signal, could not be evaluated quantitatively. Nevertheless, no change in payload performance has been observed during the two firings as well as the 50+ thruster firings performed since in-orbit commissioning.

IV. Conclusions

The Inmarsat 4F1 PPS has performed as expected throughout all the initial in-orbit testing and subsequent stationkeeping operations. The regulator, thruster and cathode combinations used during the IOT phase have ensured that all aspects of the PPS have been thoroughly checked out. The thruster behaviour has been as expected, with some outgassing at beginning of each firing showing up as current oscillations, which reduce as the firing time on each thruster is accumulated. All the thruster performances deduced from the available telemetry are consistent with the corresponding ground acceptance test data.

V. References

- ¹Gray, H., Demaire, A., and Didey, A., "Plasma Propulsion Systems For Astrium Telecommunications Satellites", AIAA-2003-6202, September 2003
- ²Stephan, J-M., "Electric propulsion activities for Eurostar 3000", 3rd International Conference on Spacecraft Propulsion, Cannes, October 2000, ESA SP-465, December 2000
- ³Cadiou, A., Gelas, C., Darnon, F., Jolivet, L. and Pillet, N, "An Overview of the CNES Electric Propulsion Program", 27th International Electric Propulsion Conference, Pasadena, California, 2001
- ⁴Stephan, J-M., Drube, M., Gray, H., and Demaire, A., "Plasma Propulsion System functional chain validation on Eurostar 3000", AIAA-2003-2408, April 2003
- ⁵Provost, S., Theroude, C., and Pezet, B., "Insight into EADS Astrium modeling packages for electric propulsion / spacecraft interactions", 4th International Spacecraft Propulsion Conference, Sardinia, June 2004
- ⁶Theroude, C., Provost, S., and Chèoux-Damas, P., "Overview of Astrium modeling tools for plasmic thruster flow-field simulation", IEPC-2003, Toulouse, March 2003
- ⁷Provost, S., Theroude, C., and Chèoux-Damas, P., "Overview of Astrium erosion / contamination modeling tool and validation on ONERA experimental results", IEPC-2003, Toulouse, March 2003
- ⁸Koppel, C., and Estublier, D., "The Smart-1 electric propulsion sub-system around the Moon: In flight experience", AIAA-2005-3670, July 2005
- ⁹Thompson, R., and Gray, H., "The Xenon Regulator and Feed System For Electric Propulsion Systems", IEPC-2005-066, November 2005